New examination of the traditional Raman Lidar technique II: temperature dependent aerosol scattering ratio and water vapor mixing ratio equations

David N. Whiteman
NASA/Goddard Space Flight Center
Greenbelt, MD 20771

January 18, 2002

Abstract

In a companion paper, the temperature dependence of Raman scattering and its influence on the Raman water vapor signal and the lidar equations was examined. New forms of the lidar equation were developed to account for this temperature sensitivity. Here we use those results to derive the temperatue dependent forms of the equations for the aerosol scattering ratio, aerosol backscatter coefficient, extinction to backscatter ratio and water vapor mixing ratio.Pertinent analysis examples are presented to illustrate each calculation. OCIS # 010.3640, 010.3920, 999.9999

1 Introduction

In part one of this paper [1] (hereafter referred to as "part I"), the effects of the temperature sensitivity of Raman scattering on the elastic and Raman lidar equations were discussed. Also a detailed examination of the calculation of atmospheric transmission was presented. Continuing with the task of re-examining the traditional Raman lidar measurements of aerosols and water vapor, in this paper is presented the temperature dependent equations for aerosol scattering ratio, aerosol backscatter coefficient and water vapor mixing ratio.

2 Aerosol scattering ratio

2.1 Definition

The backscattered lidar signal centered on the laser wavelength is caused by Rayleigh and rotational Raman scattering from air molecules and Mie scattering from aerosols. The aerosol scattering ratio is used to quantify the ratio of aerosol to molecular scattering. It is defined as the ratio of the volume backscatter coefficients β_π^{tot} for total (molecular + aerosol) scattering and pure molecular scattering and can be expressed as

$$\mathcal{R}(\lambda_L, r) = \frac{\beta_\pi^{tot}(\lambda_L, r)}{\beta_\pi^{mol}(\lambda_L, r)} = \frac{\beta_\pi^{mol}(\lambda_L, r) + \beta_\pi^{aer}(\lambda_L, r)}{\beta_\pi^{mol}(\lambda_L, r)} = 1 + \frac{\beta_\pi^{aer}(\lambda_L, r)}{\beta_\pi^{mol}(\lambda_L, r)} \tag{1}$$

where the volume backscatter coefficient for molecules $\beta_\pi^{mol}(\lambda_L, r)$ is given by $N^{mol}(r)\ d\sigma_{mol}(\pi)/d\Omega$. It is more difficult to represent the volume backscatter coefficient for aerosols as a number density multiplied by a cross section because the number density, size and type of aerosols are generally not known.

2.2 Formulation of the equations for aerosol scattering ratio

The Raman lidar is able to quantify the aerosol scattering ratio in a more direct manner than elastic lidar systems. The Raman lidar measures a signal proportional to the molecular nitrogen (or oxygen) density. This can be used as a direct quantification of the denominator needed in equation 1. A simple elastic lidar has no such signal and must resort to inversions to determine ratio.

The calculation of the aerosol scattering ratio from the basic Raman lidar signals will now be described. Forming the ratio of equations 8 and 7 from part I [1] for the background-subtracted lidar received power at the laser wavelength, λ_L, and at the Raman nitrogen wavelength, λ_N, yields

$$\frac{P(\Delta\lambda_R, r)}{P(\Delta\lambda_N, r)} = \frac{O_L(r)}{O_N(r)} \frac{F_R(T)}{F_N(T)} \frac{\xi(\lambda_L)}{\xi(\lambda_N)} \frac{\beta_\pi^{mol}(\lambda_L, r) + \beta_\pi^{aer}(\lambda_L, r)}{N_N(r) \frac{d\sigma_N(\pi)}{d\Omega}} e^{-\int_0^r \{\alpha(\lambda_L, r') - \alpha(\lambda_N, r')\} dr'} \tag{2}$$

$$= \frac{O_L(r)}{O_N(r)} \frac{F_R(T)}{F_N(T)} \frac{\xi(\lambda_L)}{\xi(\lambda_N)} \frac{\beta_\pi^{mol}(\lambda_L, r) + \beta_\pi^{aer}(\lambda_L, r)}{N_N(r) \frac{d\sigma_N(\pi)}{d\Omega}} \Delta\tau(\lambda_L, \lambda_N, r) \tag{3}$$

where the shorthand notation

$$\Delta\tau(\lambda_L, \lambda_N, r) = e^{-\int_0^r \{\alpha(\lambda_L, r') - \alpha(\lambda_N, r')\} dr'} \tag{4}$$

has been used for the differential transmission term which accounts for the fact that atmospheric transmission differs at the two wavelengths. Note the useful property that $\Delta\tau(\lambda_L, \lambda_N, r) = 1/\Delta\tau(\lambda_N, \lambda_L, r)$.

The Raman backscatter coefficient for nitrogen molecules may now be expressed as $\beta_\pi^N(\lambda_L, r) = N_N(r)\ d\sigma_N(\pi)/d\Omega$ and is proportional to the Rayleigh backscattering coefficient for air since nitrogen is well mixed in the lower atmosphere. This fact can be expressed as

$$\beta_\pi^N(\lambda_L, r) = C\, \beta_\pi^{mol}(\lambda_L, r) \tag{5}$$

The Rayleigh and Raman nitrogen cross sections, both including the rotational Raman contributions are, at 351.1 nm, approximately 3.4 $\times 10^{-27}\ cm^2 sr^{-1}$ and $3.0 \times 10^{-30} cm^2 sr^{-1}$, respectively [2]. Thus, considering also that nitrogen comprises approximately 78% of the atmosphere, C in equation 5 may be evaluated as follows

$$C \cong \frac{1}{0.78}\frac{\beta_\pi^N(\lambda_L,r)}{\beta_\pi^{mol}(\lambda_L,r)} \cong \frac{1}{0.78}\frac{3.0\times10^{-30}}{3.4\times10^{-27}} \cong 1.1\times10^{-3} \tag{6}$$

Combining equations 3 and 5, the following expression for the aerosol scattering ratio in terms of the lidar signals results

$$\mathcal{R}(\lambda_L,r) = \frac{\beta_\pi^{tot}(\lambda_L,r)}{\beta_\pi^{mol}(\lambda_L,r)} = C\,\frac{O_N(r)}{O_L(r)}\frac{F_N(T)}{F_R(T)}\frac{\xi(\lambda_N)}{\xi(\lambda_L)}\frac{P(\lambda_L,r)}{P(\lambda_N,r)}\Delta\tau(\lambda_N,\lambda_L,r) \tag{7}$$

Absorbing the overlap and efficiencies into a new term, $C^*(T,r)$, yields

$$\mathcal{R}(\lambda_L,r) = C^*(T,r)\frac{P(\lambda_L,r)}{P(\lambda_N,r)}\Delta\tau(\lambda_N,\lambda_L,r) \tag{8}$$

$$C^*(T,r) = C\,\frac{O_N(r)}{O_L(r)}\frac{F_N(T[r])}{F_R(T[r])}\frac{\xi(\lambda_N)}{\xi(\lambda_L)} \tag{9}$$

$$\cong 1.1\times10^{-3}\,\frac{O_N(r)}{O_L(r)}\frac{F_N(T[r])}{F_R(T[r])}\frac{\xi(\lambda_N)}{\xi(\lambda_L)} \tag{10}$$

For a perfect optical system, the ratio $O_N(r)/O_L(r)$ would be unity throughout the range of measurement. In a real lidar system, this ratio will depart from unity for the ranges closest to the telescope. If this departure from unity is significant for the quantity being determined, the ratio of the overlap functions can be quantified by taking data in both channels using a common nitrogen or oxygen interference filter [3] [4] (although care must be taken to use filters all of similar bandpass width since narrower filters are more subject to changes in transmission due to differing divergence angles that arise in the near-field). By doing this, both lidar system channels are measuring the same atmospheric quantity and the ratio of the data from these channels quantifies the ratio of the overlap functions.

2.2.1 Temperature sensitivity ratio $F_N(T)/F_R(T)$

Equation 10 is the Raman lidar equation for quantifying the aerosol scattering ratio using a XeF excimer laser (351 nm) such as used for the measurements by the SRL at Andros Island, Bahamas in 1998. The temperature sensitivity functions $F_R(T)$ and $F_N(T)$ appear in the final formulas and, in general, cannot be eliminated as was the case for calculating aerosol extinction in the normal atmosphere. In the calculation of extinction, $F_N(T)$ would need to change appreciably over short ranges to influence the results. In the calculation of the aerosol scattering ratio, however, any change in the value of the ratio of $F_N(T)/F_R(T)$ over the entire range of a lidar profile could affect the calibration of the profile. Thus, for high accuracy measurements of aerosol scattering ratio when using narrowband interference filters, these temperature sensitive functions should be evaluated. If the

aerosol and nitrogen filters are of essentially the same width, this factor will be minimized since the temperature dependence of the rotational-vibrational Raman lines surrounding the vibrational nitrogen q-branch is similar to that of the pure rotational Raman lines surrounding the elastic return. Furthermore, for the case of the wide spectral band SRL measurements analyzed here essentially all of the rotational lines are transmitted by the filters that were used, therefore temperature dependence was not a concern. If filters of significantly different widths are used for the elastic and Raman measurement, the factor $F_N(T)/F_R(T)$ may become important. This will be the subject of future investigation. The evaluation of the calibration constant C^* and the differential transmission term will be discussed after the error equations are developed.

2.3 Aerosol scattering ratio error equations

The standard error in determining $\mathcal{R}(\lambda_L, r)$ is given by applying the error propagation formulas, equations 28 - 31 from part I, to equation 8. The error due to the lidar signals can be quantified as follows

$$\frac{\sigma_{\mathcal{R}}^2}{\mathcal{R}^2} = \frac{\sigma_{C^*}^2}{C^{*2}} + \frac{\sigma_A^2}{A^2} + \frac{\sigma_{\Delta\tau}^2}{\Delta\tau^2} \tag{11}$$

where A has been used for the ratio of the background subtracted lidar signals, $P(\lambda_L, r)/P(\lambda_N, r)$, in equation 8. Variations in the calibration factor, C^*, and the differential transmission, $\Delta\tau$, will be studied in the next sections. It will be shown that errors in the differential transmission term can be kept small through a direct measurement of aerosol extinction. Furthermore, the atmosphere offers a natural calibration tool that permits accurate scattering ratio calibrations. Therefore, the random errors in the lidar signals themselves typically dominate the error budget. Quantifying the standard error in the aerosol scattering ratio as being determined by the random error in the lidar signals yields:

$$\frac{\sigma_{\mathcal{R}}^2}{\mathcal{R}^2} = \frac{\sigma_{SL}^2 + \sigma_{BL}^2}{(S_L - B_L)^2} + \frac{\sigma_{SN}^2 + \sigma_{BN}^2}{(S_N - B_N)^2} \tag{12}$$

$$\sigma_{\mathcal{R}}^2 = \frac{(S_L - B_L)^2}{(S_N - B_N)^2}\left(\frac{\sigma_{SL}^2 + \sigma_{BL}^2}{(S_L - B_L)^2} + \frac{\sigma_{SN}^2 + \sigma_{BN}^2}{(S_N - B_N)^2}\right) \tag{13}$$

where the subscripts L and N refer to the signals at the laser wavelength and the Raman nitrogen shifted wavelength. A point to note here is that the errors in the determination of the backgrounds, σ_{BL}^2 and σ_{BN}^2, propagate into the total error in the aerosol scattering ratio calculation.

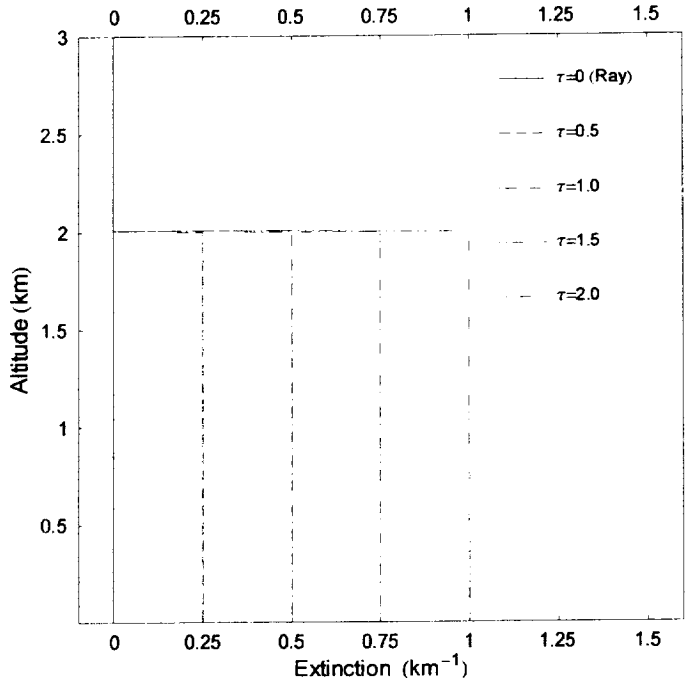

Figure 1: Five synthesized aerosol extinction profiles to test the influence of various aerosol loadings on the calculation of differential transmission. The aerosol optical depth of the profiles ranges from τ =0 (pure Rayleigh) to $\tau = 2.0$ (extremely hazy). All profiles equal 0 above 2.0 km.

2.4 Aerosol scattering ratio differential transmission

The differential transmission term $\Delta\tau\,(\lambda_N, \lambda_L, r)$ in equation 8, which accounts for the fact that the return signals at λ_L and λ_N experience different attenuations on their return trips from the scattering volume, will now be computed. The influence of various aerosol loadings on this calculation will be studied using several synthesized aerosol extinction profiles.

The synthesized profiles are shown in figure 1 where each of the profiles equals zero above an altitude of 2 km. The differential transmission term calculated using these extinction profiles is shown in figure 2 where the U.S. Standard Atmosphere [5] has been used for the molecular extinction calculation. The aerosol optical depth for each of these profiles is obtained by integrating the extinction from the 0 - 2 km. The aerosol optical depths, τ, that result are shown in the legend of the figure. They range from a pure Rayleigh atmosphere ($\tau = 0$) to an extremely hazy value of $\tau = 2.0$. In these plots, the Angstrom coefficient used was $k =$ 1.0.

For a moderately turbid value of aerosol optical depth of 0.5, the differential transmission term changes by less than 5% at

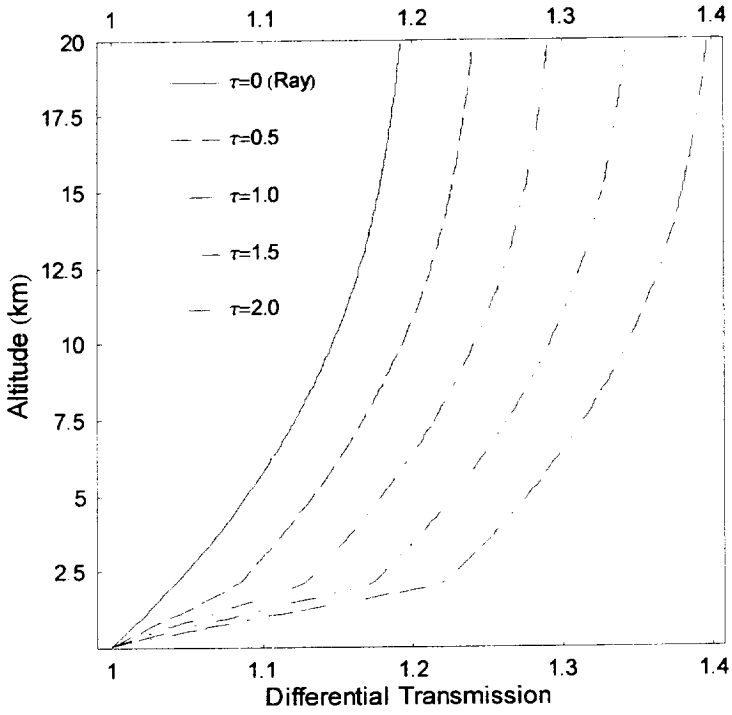

Figure 2: The differential transmission term required for the aerosol scattering ratio calculation for a range of optical depths. Increasing the optical depth makes the differential transmission term larger with height. $\tau = 0$ indicates only molecular scattering while $\tau = 2.0$ would indicate very hazy conditions. The standard atmosphere has been to calculate the molecular extinction.

20 km from the pure Rayleigh value. However, under the extremely hazy conditions of an aerosol optical depth of 2.0, the value of the differential transmission term increases to almost 1.4 at 20 km from its pure Rayleigh value of approximately 1.15. The differential transmission curves are essentially parallel to each other above 2 km, as expected, since the aerosols are confined to a region below 2 km in the synthetic profiles. This figure shows the importance, particularly under hazy conditions, of having a simultaneous measurement of aerosol extinction.

The value chosen for the Angstrom coefficient influences the calculation of the differential transmission term as shown in figure 3. Varying the Angstrom coefficient over a range of 0.8 to 1.2 for the case of aerosol optical depth of 1.0 changes the differential transmission term by 4%. Thus, under very hazy conditions, a knowledge of the wavelength scaling of the aerosols present, such as can be obtained by sun photometer, can help to reduce the uncertainty in this term. (However, a sun photometer only yields the column average Angstrom coefficient. A multi-wavelength lidar [6] [7] can be used to quantify the Angstrom coefficient as a function of range but that is beyond the scope of the present treatment, which is confined to a single output laser wavelength.) The use of the molecular oxygen signal, as opposed to the molecular nitrogen signal used here, will also decrease this sensitivity due to the fact that the Raman shifted wavelength for oxygen is closer to the laser wavelength than is the Raman shifted wavelength for nitrogen.

2.5 Atmospheric calibration of the aerosol scattering ratio

The atmosphere offers a natural calibration tool for determining the factor $C^*(T,r)$ in equation 8. After correcting for differential transmission as shown above, $C^*(T,r)$ may be determined by examining the lidar quantity $P(\lambda_L,r)/P(\lambda_N,r)\ \Delta\tau(\lambda_N,\lambda_L,r)$ from equation 8 in a region of the atmosphere which is free of aerosols. The functions $F_N(T)$ and $F_R(T)$ must be known over the range of the profile to apply the calibration constant at all altitudes. If wideband filters are used, such as in the SRL excimer based measurements, these functions are essentially constant implying that $C^*(T,r)$ is a constant for all temperatures. For the case of narrowband filters, this may not be the case as mentioned earlier.

In non-volcanic conditions, Russell et. al. [8] [9] demonstrate that there are very few aerosols present in the free troposphere (above the boundary layer but below the tropopause). They show that the minimum value of aerosol scattering ratio $\mathcal{R}_{min}(\lambda)$ for a wavelength of 690 nm is not greater than 1.02. Using this value of $\mathcal{R}_{min}(\lambda)$ and a λ^{-4} dependence for Rayleigh scattering and assuming a λ^{-k} dependence in aerosol scattering coefficient (considered constant as a function of range) implies that at the XeF excimer wavelength of 351.1 nm the correct value of $\mathcal{R}_{min}(\lambda)$ can be determined in the following manner.

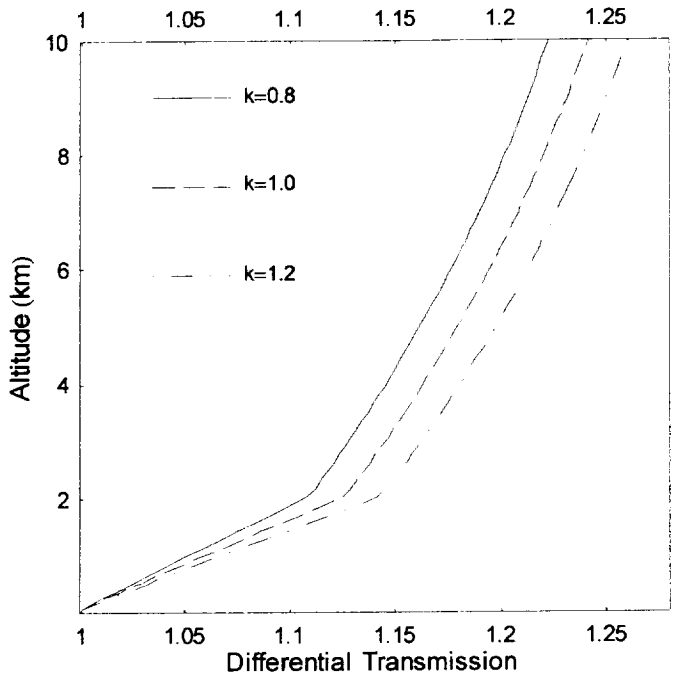

Figure 3: The sensitivity of the aerosol scattering ratio differential transmission term to the wavelength scaling of aerosol extinction is tested here. For an aerosol optical depth of 1.0, the aerosol differential transmission term is plotted for $k = 0.8$, 1.0 and 1.2. The differential transmission term changes by approximately 4% over this range.

The wavelength scaling of the Rayleigh and Mie backscattering coefficients may be expressed as

$$\frac{\beta_\pi^{mol}(\lambda_1, r)}{\beta_\pi^{mol}(\lambda_2, r)} = \left(\frac{\lambda_2}{\lambda_1}\right)^4 \tag{14}$$

$$\frac{\beta_\pi^{aer}(\lambda_1, r)}{\beta_\pi^{aer}(\lambda_2, r)} = \left(\frac{\lambda_2}{\lambda_1}\right)^k \tag{15}$$

Given that the aerosol scattering ratio at wavelength λ_1 is

$$\mathcal{R}(\lambda_1, r) = 1 + \frac{\beta_\pi^{aer}(\lambda_1, r)}{\beta_\pi^{mol}(\lambda_1, r)} \tag{16}$$

equations 14 and 15 can now be used in conjunction with equation 1, the expression for aerosol scattering ratio, to scale the scattering ratio to different wavelengths. Therefore, at λ_2 the following equation pertains

$$\mathcal{R}(\lambda_2, r) = 1 + \frac{(\lambda_1/\lambda_2)^k \ \beta_\pi^{aer}(\lambda_1, r)}{(\lambda_1/\lambda_2)^4 \ \beta_\pi^{mol}(\lambda_1, r)} = 1 + \frac{\beta_\pi^{aer}(\lambda_1, r)}{(\lambda_1/\lambda_2)^{4-k} \ \beta_\pi^{mol}(\lambda_1, r)} \tag{17}$$

Using now the values of $\lambda_1 = 690\ nm$, $\lambda_2 = 351.1\ nm$, $\mathcal{R}_{min}(690, r) = 1.02$, and $k = 1$ yields $\mathcal{R}_{min}(351.1, r) = 1.0026$. The Angstrom coefficient, k, generally varies between the extremes of approximately 0 and 2. Even assuming the maximum value of $k = 2$, $\mathcal{R}_{min}(351.1, r) = 1.005$. Due to the very small value of $\mathcal{R}_{min}(\lambda = 351.1, r)$ for all values of k, the calibration of the aerosol backscattering ratio can be performed by assuming that the minimum value of backscattering ratio that a Raman lidar measures between 6 and 10 km corresponds to an aerosol backscattering ratio of 1.0. The error in this assumption is much less than 1%.

The determination of the value of aerosol scattering ratio from equation 8 is illustrated in figure 4 using SRL data acquired during the night of August 22, 1998 at Andros Island. A 10-minute summation of the ratio of the aerosol and nitrogen channels, $P(\lambda_L, r)/P(\lambda_N, r)$ is plotted in solid black. The profile slopes toward smaller values as altitude increases due to the differential transmission of the two lidar wavelengths; 351.1 nm for aerosol and 382.3 nm for nitrogen. Multiplying by the differential transmission term $\Delta\tau(\lambda_N, \lambda_L, r)$ in equation 8 yields the curve shown using a dashed line. $C^*(T, r)$ can now be determined by normalizing the profile to a value of 1.0 in an aerosol-free value region of the atmosphere. As described above, the region between 6 - 10 km is used for this normalization. The dash-dot curve then is the fully processed aerosol backscattering ratio $\beta_\pi^{tot}(\lambda_L, r)/\beta_\pi^R(\lambda_L, r)$ with errors calculated using equation 12. In the profiles, one can see small amounts of aerosol scattering

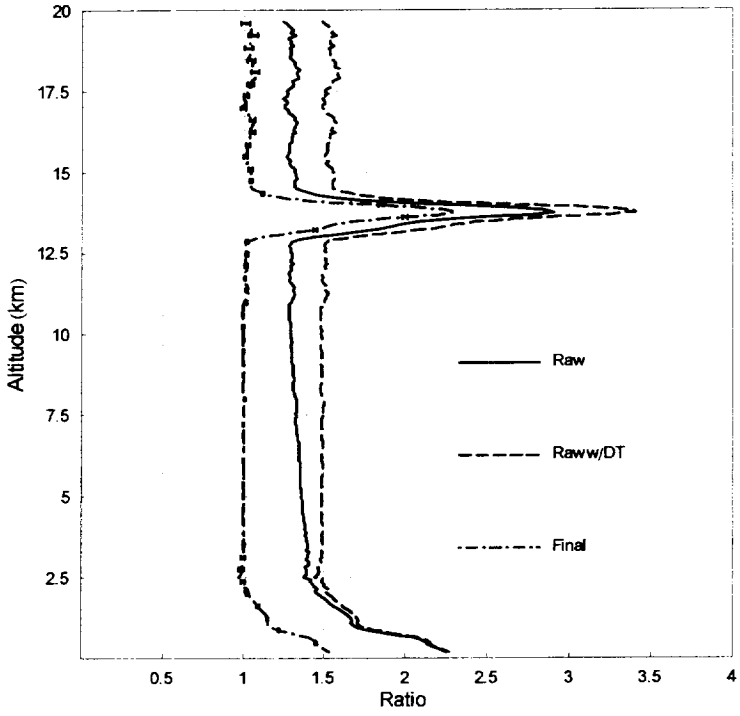

Figure 4: The steps in the evaluation of equation 8 are shown. In solid line is shown the raw ratio of the lidar signals $P(\lambda_L, r)/P(\lambda_N, r)$. The dashed curve is the same ratio after multiplying by the differential transmission term $\Delta\tau(\lambda_N, \lambda_L, r)$ calculated from equation 8 using actual lidar aerosol extinction data and molecular number density from a radiosonde. Finally the value of C^* is determined by normalizing the curve between 6 - 10 km where aerosol scattering is negligible. The final curve is the fully processed aerosol backscattering ratio given by $\beta_\pi^{tot}(\lambda_L, r)/\beta_\pi^R(\lambda_L, r)$.

present near the surface with scattering ratios reaching ~1.5. Cirrus clouds can be seen between 13 - 14 km where the values are greater than 2.

From this example, $C^*(T,r)$ has a constant value of approximately 0.65. This value shows no range dependence due to the wide interference filters in use. In equation 10, the overlap and temperature sensitivity ratios will both be approximately equal to one. Thus, the value of $C^*(T,r)$ implies that the ratio of transmission efficiencies, $\xi(\lambda_N)/\xi(\lambda_L)$, must be on the order of 10^3. In fact, these data were acquired with an ND3 (transmission =10^{-3}) neutral density filter installed in the elastic channel to allow the signal to be acquired using photon counting electronics. The aerosol backscattering coefficient can be calculated from the aerosol scattering ratio. In order to do this, the Rayleigh backscatter cross section is needed. That calculation will now be described.

2.6 Calculation of Rayleigh backscatter cross section

To calculate the Rayleigh backscatter cross section, the following formulation will be used [10]

$$\beta^{mol}(\theta,\lambda,z) = \frac{\beta_s(\lambda,z)}{4\pi} P_{Ray}(\theta,\gamma(\lambda)) \tag{18}$$

where $\beta^{mol}(\theta,\lambda,z)$ is the Rayleigh angular volume-scattering coefficient (in units of, for example, $cm^{-1}sr^{-1}$).The right hand side of this equation consists of two terms indicating: 1) total scattering per molecule and 2) scattering amplitude in a given angular direction. The $\beta_s(\lambda,z)$ term is the same Rayleigh volume scattering coefficient given in equation 17 of part I and quantifies scattering into all angles. The angular dependent part is given by [10]

$$P_{Ray}(\theta,\gamma(\lambda)) = \frac{3}{4(1+2\gamma(\lambda))}\left[(1+3\gamma(\lambda)) + (1-\gamma(\lambda))\cos^2\theta\right] \tag{19}$$

where $P_{Ray}(\theta,\gamma)$ is the Rayleigh scattering phase function and γ quantifies molecular anisotropy and is defined by

$$\gamma(\lambda) = \frac{\rho_n(\lambda)}{2-\rho_n(\lambda)} \tag{20}$$

where $\rho_n(\lambda)$ is the Rayleigh depolarization factor shown in figure 4 of part I. This formulation of the Rayleigh scattering phase function is due to Chandrasekhar [11]. The Rayleigh backscattering cross section is obtained simply by setting $\theta = \pi$ in the equations 18 and 19.

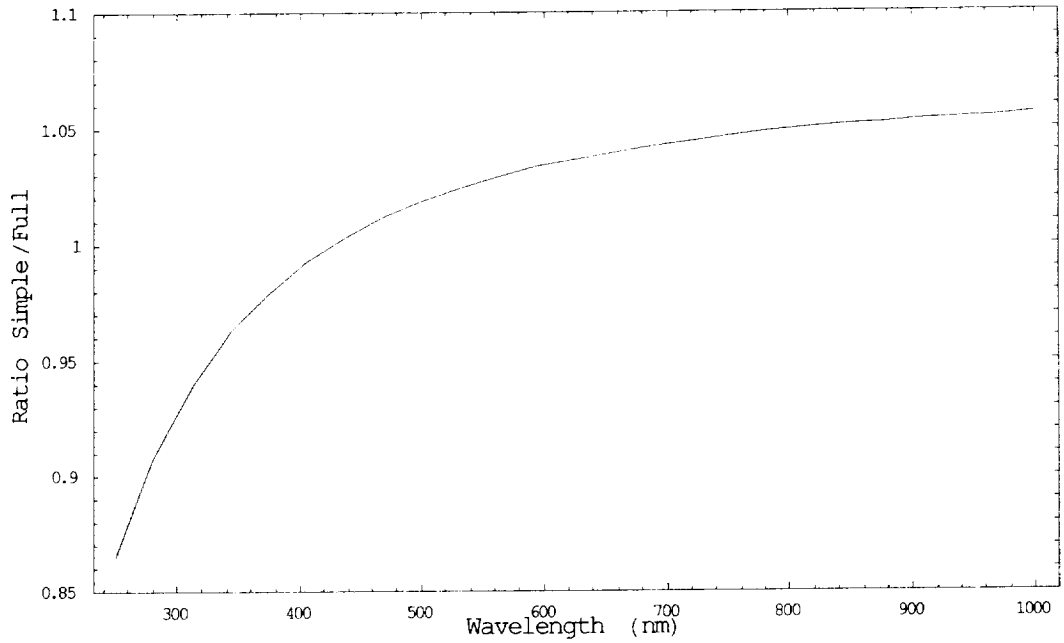

Figure 5: The ratio of two formulations of the Rayleigh backscatter coefficient, given by equations 21 and 18, is plotted from 250 to 1000 nm. This plot shows the importance of including the dispersion of the depolarization in calculations of Rayleigh backscattering.

It is interesting to compare this formulation of Rayleigh backscattering to a simpler numerical version that is often used but that does not account for the effects of the dispersion of depolarization. The simpler equation may be expressed as [2]

$$\beta_{\pi}^{simpler}(\lambda) = N\,\sigma_{\pi}^{R}(\lambda) = N\,5.45\left[\frac{550}{\lambda(nm)}\right]^{4} \times 10^{-28} \quad (cm^{-1}sr^{-1}) \tag{21}$$

where N is the molecular number density and $\sigma_{\pi}^{R}(\lambda)$ is the Rayleigh backscatter cross section. Figure 5 shows the ratio of equations 21 and 18 over a range of 250 to 1000 nm where the latter equation has been evaluated at an angle of π.

The non-constant ratio shown in the plot is due to the different methods of calculating the Rayleigh cross section. The full method shown in equation 18 includes the dispersion of the depolarization ratio and should be used when high accuracy is required. The two methods differ by more than 10% for wavelengths shorter than approximately 280 nm and by more than 5% for wavelengths greater than approximately 800 nm. At the wavelength in use here of 351 nm, the difference is ~3%. Again it should be noted that the dispersion of depolarization shown in the figure includes the full effects of rotational Raman scattering.

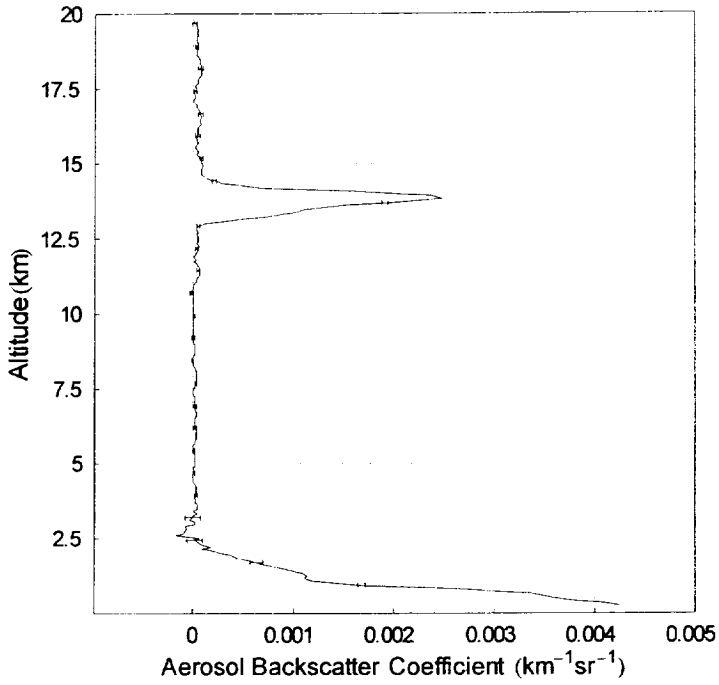

Figure 6: Aerosol backscattering coefficient calculated on the night of August 22, 1998. Tropospheric aerosols can be seen up to altitudes of approximately 3 km while a cirrus cloud layer is apparent between 13 and 15 km.

2.7 Aerosol backscattering coefficient

Using the Rayleigh backscatter cross section shown in equation 18, the aerosol backscatter coefficient is easily determined from the aerosol scattering ratio as follows.

$$\beta^{aer}(\lambda_L, z) = \beta^{mol}(\pi, \lambda_L, z)\left(\mathcal{R}(\lambda_L, z) - 1\right) \tag{22}$$

Figure 6 shows the aerosol backscatter coefficient corresponding to the aerosol scattering ratio given in figure 4. The errors plotted are those due to the random error in the aerosol scattering ratio given by equation 12 and do not include any error contribution due to the knowledge of the molecular number density.

In terms of backscatter coefficient, which gives the intensity of light back-scattered per incident photon, the tropospheric aerosols yield higher values than the cirrus cloud. In terms of the aerosol scattering ratio given in figure 4, however, the scattering ratio of the cloud is larger than that for the tropospheric aerosols. So, although the cirrus cloud has a lower probability of

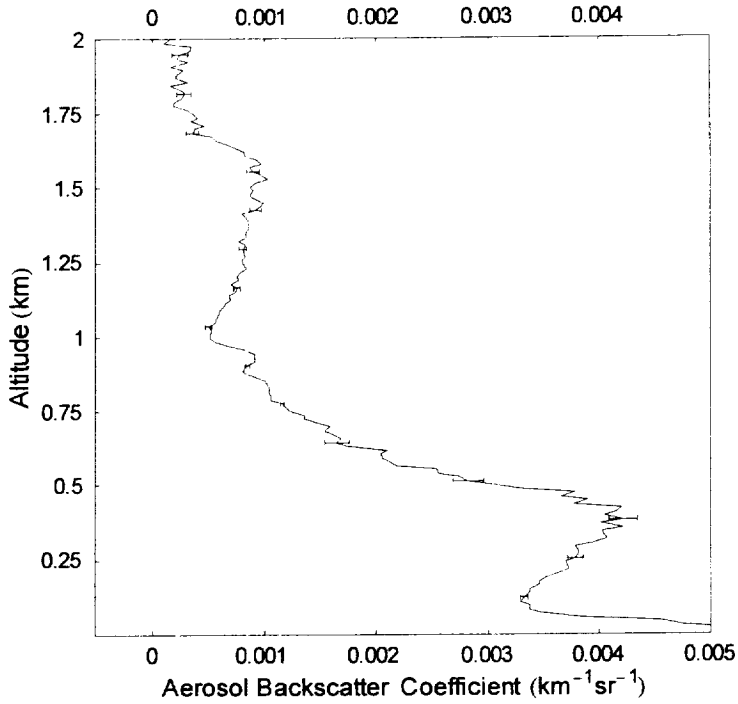

Figure 7: Aerosol backscatter coefficient for the tropospheric aerosols that were present during the night of August 26, 1998 at Andros Island. Data acquired at a low elevation angle have been used to improve the measurement of extinction.

backscattering an incident photon than does the tropospheric aerosol layer, the ratio of scattering from the cirrus clouds to the scattering by molecules at the height of cirrus cloud is greater than the corresponding ratio for the tropospheric aerosols.

2.8 Extinction to backscatter ratio

The ratio of aerosol extinction to backscatter is an important optical parameter that can yield information about the physical nature of the aerosol [12]. For example, quantification of this ratio is useful in studying the growth of aerosols as a function of relative humidity [13]. The aerosol backscatter data from August 26, 1998 corresponding to the extinction data presented in figure 6 of part I are shown in figure 7. Data acquired at an angle of 10 degrees up from the horizon were used from this night to improve the vertical resolution.

In general during the CAMEX-3 campaign, the top of the marine boundary layer (MBL) was observed to be at ~1 km as indicated by a roughly constant water vapor mixing ratio. On the night of August 26, the marine boundary layer height was again at approximately 1 km. A signature can be seen in the aerosol data at this altitude which likely indicates the top of the marine

boundary layer. Above this, the backscattering due to aerosols increases slightly, which is consistent with a change in aerosol composition. This same signature can be seen in the extinction to backscatter ratio. This ratio is formed using the data shown in figure 6 of part I and figure 7 here. The result is plotted in figure 8. The error bars plotted for the ratio are determined using equation 30 from part I. The relative decrease in extinction to backscatter ratio above 1 km is another indication of a change in aerosol type. This could be an indication of different aerosol types that have been transported aloft as opposed to local aerosols that swelled within the marine boundary layer.

The increase in extinction to backscatter ratio up to an altitude of 1 km, the height of the marine boundary layer, could be an indication of aerosol swelling. This is often seen as height increases inside a well-mixed boundary layer. Aerosols begin to swell when the relative humidity increases above ~70% [14]. Since a well-mixed boundary layer should have a relatively constant mixing ratio and mixing ratio is a conserved quantity, as a parcel of air cools within the boundary layer, the relative humidity of the parcel will increase. Atmospheric temperature typically decreases with altitude, thus the relative humidity is often seen to increase with altitude in the boundary layer. When the relative humidity exceeds ~70%, one can expect aerosol swelling to commence. An increase in the aerosol size due to hygroscopic growth increases the forward-scattering more than it increases the backward scattering. In general, the result of this is to increase the particle extinction at the expense of backscattering thus increasing the ratio. Thus, the increase in the extinction to backscatter ratio between 0.5 km and 1.0 km is consistent with aerosol swelling due to increases in relative humidity above the threshold 70% value. In fact, measurements of atmospheric relative humidity made by an Atmospheric Emitted Radiance Interferometer (AERI) [15] at the same time as these lidar measurements indicated that relative humidities exceeded 70% between approximately 0.4 km and 1.1 km supporting the conclusion that the increase in extinction to backscatter ratio below 1.0 km is due to aerosol growth.

3 Water vapor mixing ratio

3.1 Definition

Water vapor is one of the most important atmospheric state variables. The profile of water vapor in the atmosphere determines convective atmospheric stability which influences whether storm initiation is likely. It also is the most active greenhouse gas; it absorbs terrestrial radiation more strongly than CO_2. The ratio of the mass of water vapor to the mass of dry air in a given

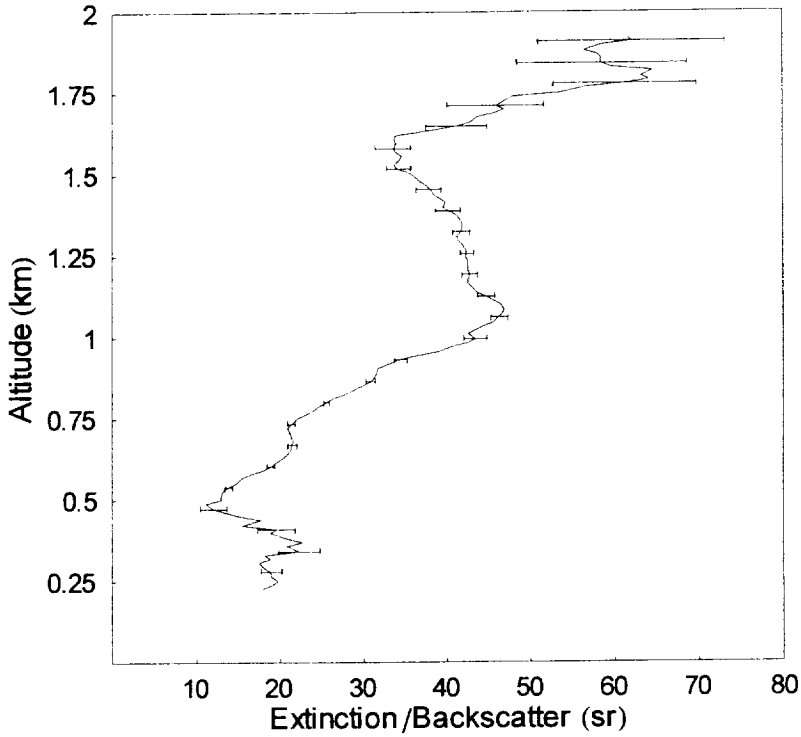

Figure 8: Aerosol extinction to backscatter ratio using a 20 minute summation of data on the night of August 26, 1998 in Andros Island, Bahamas.

volume, known as the water vapor mixing ratio, is a convenient way to quantify the amount of water vapor in the atmosphere. The mixing ratio is conserved in atmospheric processes that do not involve condensation or evaporation and thus serves well as a tracer of the movement of air parcels in the atmosphere.

3.2 Calculation of the water vapor mixing ratio from the lidar equation

Using equation 8 from part I for single scattering Raman lidar measurements of water vapor and nitrogen, respectively, the ratio of these two signals, including the effects of temperature sensitivity, becomes

$$\frac{P(\lambda_H, r)}{P(\lambda_N, r)} = \frac{O_H(r)\ F_H(T)\ N_H(r)\ \frac{d\sigma_H(\pi)}{d\Omega}\ \xi(\lambda_H)}{O_N(r)\ F_N(T)\ N_N(r)\ \frac{d\sigma_N(\pi)}{d\Omega}\ \xi(\lambda_N)} e^{-\int_0^r \{\alpha(\lambda_H, r') - \alpha(\lambda_N, r')\} dr'} \tag{23}$$

The exponential factor expresses the difference in one-way atmospheric transmission between Raman wavelengths and will be abbreviated $\Delta\tau(\lambda_H, \lambda_N, r)$ following the shorthand convention of equation 4.

Recalling that the water vapor mixing ratio is the ratio of the mass of water vapor and the mass of dry air, and considering that nitrogen forms a constant fraction (~0.78) of "dry air" in the lower atmosphere, it is apparent that

$$w = \frac{MW_{H_2O}}{MW_{DryAir}} \frac{N_H(r)}{N_{DryAir}(r)} \cong \frac{MW_{H_2O}}{MW_{DryAir}} \frac{N_H(r)}{N_N(r)/0.78} \cong 0.485 \frac{N_H(r)}{N_N(r)} \tag{24}$$

where w is the water vapor mixing ratio, MW_{H_2O} is the molecular weight of water vapor (18 $g/mole$), MW_{Air} is the molecular weight of "dry air" (an averaged quantity whose value is ~28.94 $g/mole$ [16]). Combining equation 23 and 24 yields

$$w = k \frac{O_N(r)}{O_H(r)} \frac{F_N(T)}{F_H(T)} \frac{P(\lambda_H, r)}{P(\lambda_N, r)} \frac{\frac{d\sigma_N(\pi)}{d\Omega}}{\frac{d\sigma_H(\pi)}{d\Omega}} \frac{\xi(\lambda_N)}{\xi(\lambda_H)} \Delta\tau(\lambda_N, \lambda_H, r) \tag{25}$$

using the fact that $\Delta\tau(\lambda_N, \lambda_H, r) = 1/\Delta\tau(\lambda_H, \lambda_N, r)$ and representing the constant of proportionality in equation 24 as k ($\cong 0.485$).

In practice, ratio measurements using the SRL are influenced by a non-unity overlap function, $O_N(r)/O_H(r)$, within the first ~0.3 km. This may be corrected using the nitrogen filter technique mentioned in section 2.2. Another technique that can be used to reduce the influence of the overlap function is to use the scanning capability of the instrument and acquire data at a low elevation angle, assume horizontal homogeneity over the atmosphere within a few kilometers of the lidar location, and convert the angle data to vertical data. This limits the influence of the lidar overlap functions to approximately the lowest 10-50 meters

for the calculation of the water vapor mixing ratio. Above this point, $O_N(r)/O_H(r)$ may be then considered to be constant and equal to unity. Using either of these approaches, above some point in the vertical profile, which can be as little as 10-50 m above the lidar site, the overlap functions no longer have an influence.

The water vapor mixing ratio equation can now be expressed using a single calibration factor as follows

$$w = k^*(T,r)\frac{P(\lambda_H,r)}{P(\lambda_N,r)}\Delta\tau(\lambda_N,\lambda_H,r) \tag{26}$$

$$k^*(T,r) \cong 0.485\frac{O_N(r)}{O_H(r)}\frac{F_N(T[r])}{F_H(T[r])}\frac{3.0\times10^{-30}}{6.0\times10^{-30}}\frac{\xi(\lambda_N)}{\xi(\lambda_H)} \tag{27}$$

$$\cong 0.24\frac{O_N(r)}{O_H(r)}\frac{F_N(T[r])}{F_H(T[r])}\frac{\xi(\lambda_N)}{\xi(\lambda_H)} \tag{28}$$

where $k^*(T,r)$ is now the lidar system calibration factor and the values for the Raman nitrogen and water vapor cross sections at 351 nm, calculated using values at 690 nm [2] and accounting for the ν^4 scaling of molecular scattering, have been used.

3.2.1 Temperature sensitivity ratio $F_N(T)/F_H(T)$

As in the case of the aerosol scattering ratio calculation, the temperature dependent functions $F_N(T)$ and $F_H(T)$ must be evaluated to apply the calibration throughout the profile. The calculation of $F_H(T)$ has already been illustrated. $F_N(T)$ can be calculated using modeling of the rotational-vibrational line strength [17] and knowledge of the lidar system spectral bandpass for the nitrogen channel. The ratio of these two temperature sensitivities yields the final temperature sensitivity of the measurement. This will be the subject of a future investigation. However, due to the large contrast between the intensity of the central q-branch of N_2 and the vibration-rotation lines, the function $F_N(T)$ is anticipated to show little variation with temperature for most real filters. The temperature dependence of the ratio $F_N(T)/F_H(T)$ should therefore be dominated by that of $F_H(T)$. For the wide spectral filters used to acquire the data analyzed here, the overall temperature dependence is small and $k^*(T,r)$ can be considered constant outside of the overlap region. The error equations for the mixing ratio will now be formulated.

3.3 Water vapor mixing ratio error equations

The standard error in determining w is given by applying the error propagation formulas, equations 28 - 31 from part I, to equation 26. The result is

$$\frac{\sigma_w^2}{w^2} = \frac{\sigma_{k^*}^2}{k^{*2}} + \frac{\sigma_{R_w}^2}{R_w^2} + \frac{\sigma_{\Delta\tau}^2}{\Delta\tau^2} \tag{29}$$

where the abbreviation $R_w = P(\lambda_H, r)/P(\lambda_N, r)$ has been used. The full quantification of equation 29 requires analysis of the variation of all factors that go into the calibration of the water vapor mixing ratio. The Raman lidar calibration has been shown to be very stable over periods of years [18] thus the variance in k^* will be considered to be very small. Errors introduced by uncertainties in the water vapor mixing ratio differential transmission term will be studied in the next section where it will be shown that, by using the Raman lidar measurement of aerosol extinction, error in this term can be kept very small also. Thus errors due to fluctuations in the ratio of the lidar signals themselves usually dominate the error budget. They will now be quantified using Poisson statistics.

Recalling that the P terms in equation 26 are actually background subtracted quantities, $\sigma_{R_w}^2/R_w^2$ may be re-expressed using the following abbreviations $P(\lambda_H, r) = S_H - B_H$ and $P(\lambda_N, r) = S_N - B_N$ where S refers to the laser induced signals and B refers to the background terms as follows

$$\frac{\sigma_{R_w}^2}{R_w^2} = \frac{\sigma_{SH}^2 + \sigma_{BH}^2}{(S_H - B_H)^2} + \frac{\sigma_{SN}^2 + \sigma_{BN}^2}{(S_N - B_N)^2} \tag{30}$$

$$\sigma_{R_w}^2 = \frac{(S_H - B_H)^2}{(S_N - B_N)^2}\left(\frac{\sigma_{SH}^2 + \sigma_{BH}^2}{(S_H - B_H)^2} + \frac{\sigma_{SN}^2 + \sigma_{BN}^2}{(S_N - B_N)^2}\right) \tag{31}$$

where it is explicitly shown that there is error in the determination of the backgrounds. Under certain conditions, such as high background during daytime measurements, these error source can become significant.

3.4 Water vapor mixing ratio differential transmission

Figure 9 shows the water vapor mixing ratio differential transmission term, $\Delta\tau(\lambda_N, \lambda_H, r)$, for the range of aerosol optical depths shown in figure 1 where a value of 1.0 was used for the Angstrom coefficient. The 1976 U. S. Standard Atmosphere [5] was used to calculate the molecular component of the extinction.

For a pure Rayleigh atmosphere, the value of the water vapor differential transmission varies from 1 at the surface to approximately 0.93 at 20 km. For an aerosol optical depth of 0.5 the range of values increases to 1.0 - 0.91. As aerosol loading increases, the differential transmission term becomes smaller. Notice that the curves are all parallel above 2 km. As in the case for aerosol scattering ratio calculations studied earlier, the part of the differential transmission that is due to aerosols is confined to the lowest

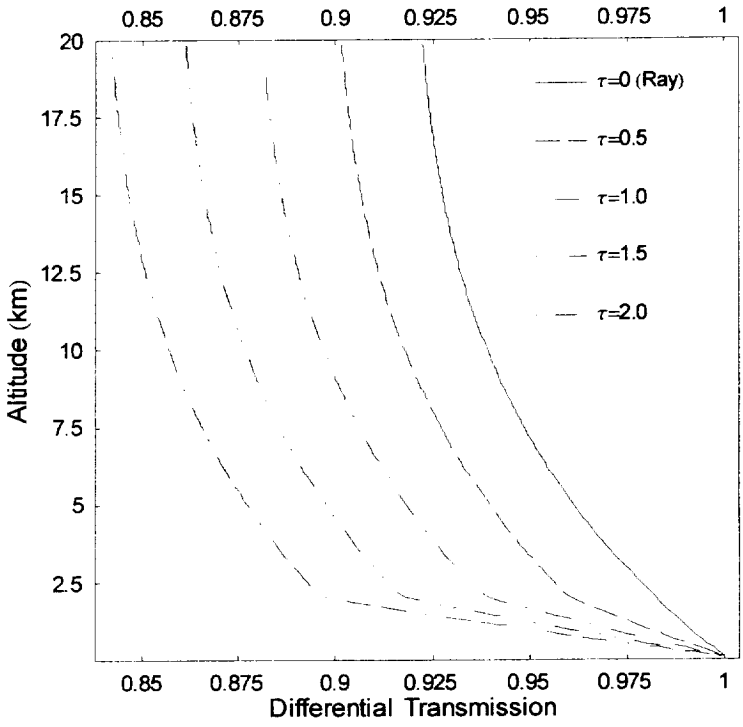

Figure 9: Differential transmission term for the calculation of water vapor mixing ratio using various modeled aerosol loadings ranging from a pure Rayleigh atmosphere to extremely hazy ($\tau = 2.0$). Changes in aerosol optical depth of 0.5 introduce a change in the differential transmission term of approximately 2%.

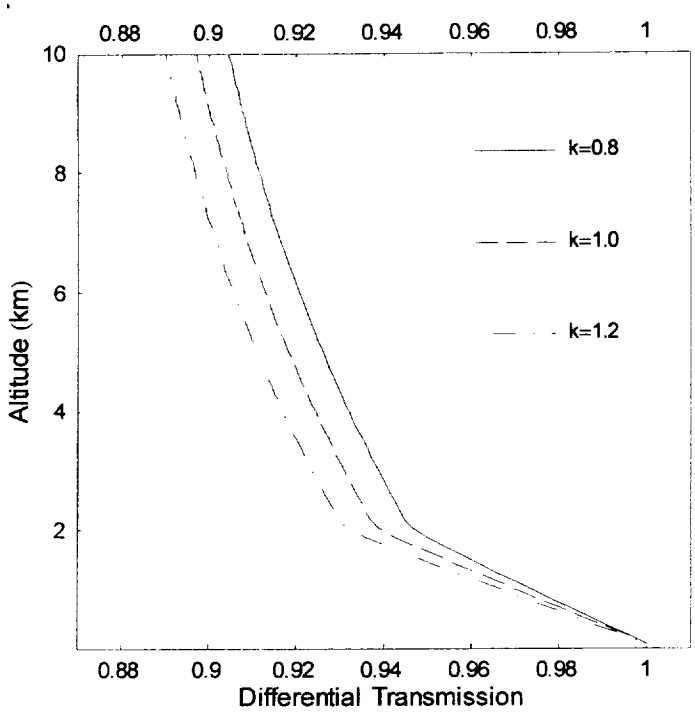

Figure 10: Differential tranmission term using an aerosol optical depth and allowing Angstrom coefficient to vary between 0.8 and 1.2. The differential transmission term changes by less than 2% over this range of k.

2 km.

Since the Raman lidar can be used to measure the round-trip aerosol extinction directly, actual lidar profiles of aerosol extinction can be used to generate the required differential transmission term. However, there still remains the uncertainty in what value of k to use in the calculation of the one-way aerosol extinction. As shown in figure 6 of part I, varying k influences the derived extinction. This is why additional aerosol information such as provided by a sun photometer is useful in this analysis. To test the sensitivity of the differential transmission to changes in the Angstrom coefficient, k, for an upward looking system, figure 10 was generated using various values of k for an aerosol optical depth of 1.0. Varying k from 0.8 to 1.2 causes only a 2% change in the differential transmission.

3.5 Raman lidar water vapor mixing ratio calibration

The issue of lidar calibration is a very important one since this is the process that leads to useful meteorological quantities. There are two approaches that have been taken in the effort to calibrate the water vapor measurements of a Raman lidar system: 1) a

first principles calibration that accounts for the total efficiency of transmitting photons through the atmosphere, scattering them off of the molecules of interest and then detecting them with the lidar receiver system, and 2) by comparison with another water vapor sensor such as a radiosonde or a microwave radiometer.

3.6 First principles water vapor calibration

An early effort to calibrate a Raman water vapor lidar system was described by Vaughan et. al. [3]. Their system was a simple two-channel lidar system which used a non-dichroic beamsplitter to share power between the water vapor and nitrogen PMTs. Their approach was to use a nitrogen filter in front of both PMTs simultaneously. This allowed the relative efficiencies of the PMTs and the power splitter to be determined. They then determined the optical efficiency of their collimating optics for each of the wavelengths. The largest uncertainty in the calibration procedure was in the knowledge of the Raman backscatter cross sections for water vapor and nitrogen. The value that they used for the ratio of the water vapor and nitrogen Raman cross sections was 2.5 $\pm$ 10% [19] (assuming nitrogen q-branch selection). Including the other uncertainties in their calibration procedure, the total uncertainty cited by these authors amounted to about 12%. A recent and much more thorough effort of absolute calibration [20] achieved a total error of 12-14%. The uncertainty in the Raman water vapor cross section was the dominant source of error in both of these absolute calibration efforts. More work needs to be done to improve the knowledge of the absolute value of the Raman cross section of water vapor. Until it is better known, calibration with respect to other water vapor sensors is likely to remain popular since the total error of the measurement can be lower using this technique.

3.7 Calibration with respect to radiosonde and other water vapor sensors

It has been demonstrated [18] that the SRL can maintain a mean calibration with less than 5% variation over several years when the calibration is derived from an ensemble of selected radiosonde measurements. Long-term calibration of a Raman water vapor lidar with respect to microwave radiometer [21] has also been performed with the same result that the mean calibration varies by much less than 5% if no changes are made in the lidar system.

The final SRL calibration constant for the CAMEX-3 campaign was derived in two ways that resulted in nearly identical values. One was through the use of 31 radiosonde comparisons, the other was by using a set of measurements made at the base of low altitude cumulus clouds and assuming that saturation obtained at cloud base [22]. One of the radiosonde comparisons will now be shown to illustrate the radiosonde calibration technique.

To determine the calibration constant with respect to a single radiosonde, the quantity on the right hand side of equation 26, $k^* P(\lambda_H, r) / P(\lambda_N, r) \ \Delta\tau(\lambda_N, \lambda_H, r)$, must be compared as a function of height to a simultaneous radiosonde measurement. The parameter k^* is adjusted to achieve a best fit with the radiosonde data over a range where both instruments are yielding good data. In the case of the lidar, this means, for example, above the altitude where the system overlap function is an influence; for the radiosonde, this typically means measurements outside of clouds and with temperatures above -40 C. For some earlier radiosonde measurements, it was necessary to select for relative humidity values above 20% [23] [18] [24] although most radiosondes can now report values well below 20%.

Figure 11 shows a lidar/radiosonde comparison from the night of August 22, 1998 at Andros Island during CAMEX-3. The best fit between a 10-minute lidar profile and the radiosonde was determined between the heights of 1 - 3 km. The calibration constant, k^*, determined from this comparison was ~0.204. Using this value of k^* in equation 26 produces the lidar water vapor mixing ratio in units of kg of water vapor per kg of dry air. The units of mixing ratio typically used in these plots, however, are grams of water vapor per kilogram of dry air (g/kg) which is obtained by multiplying by 1000. It is interesting to note that the calibration value of .204 indicates that, using equation 28, the ratio of lidar system efficiencies, $\xi(\lambda_N) / \xi(\lambda_H) = 0.204/0.24 \cong 0.85$. In other words, the SRL optical detection system has ~15% higher efficiency in the water vapor channel than in the nitrogen channel; this was the result of an optical design which maximized the transmission of the water vapor wavelength at the expense of the other (stronger) signals such as nitrogen.

The data are shown in the figure both on a linear scale on the left and on a log scale on the right. The linear scale shows the discrepancy between the lidar and the radiosonde in the first kilometer with the radiosonde showing a low-level moisture inversion. This may be a real event in the atmosphere or it could also be an indication that the radiosonde required some time to equilibrate to the environment [25]. The log scale on the right shows the good agreement of the two sensors in the upper regions of the profile where mixing ratio values are very small. The lidar data on the left are plotted with 75 m vertical resolution. The lidar data on the right use 75 m resolution up to 6 km, 225 m resolution between 6 - 8 km and 375 m above 8 km.

4 Summary

As the second part of a two-part review of the traditional Raman lidar measurements of water vapor and aerosols, the temperature dependent forms of the lidar equations developed in part I [1] have then used to derive equations for the aerosol scattering ratio,

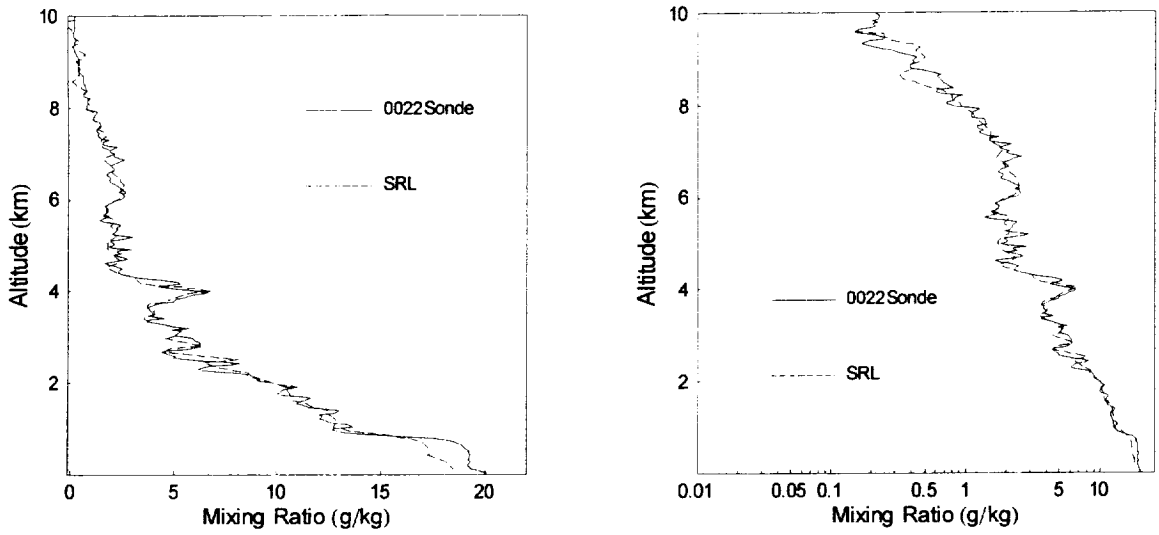

Figure 11: Comparison of a 10-minute SRL water vapor mixing ratio profile with that of a coincidently launched radiosonde with a linear scale on the left and a log scale on the right. The SRL water vapor calibration was determined through a best fit procedure between the lidar and the radiosonde between 1 - 3 *km*. The radiosonde was launched at 0022 or 0.37 UT.

aerosol extinction, aerosol backscatter coefficient and the water vapor mixing ratio. The appropriate error equations were also derived for these quantities. It was shown that not including the depolarization of Rayleigh scattering can have a quite significant effect on the calculation of the backscatter coefficient. The calculation of the differential transmission term was treated carefully and the influence of the wavelength scaling of aerosols was examined. Pertinent analysis examples were shown in each case.

5 Acknowledgements

Support for this activity has come from the NASA Dynamics and Remote Sensing and Radiation Sciences programs as well as the Department of Energy's Atmospheric Radiation Measurements program.

6 References

[1] D. N. Whiteman, "New examination of the traditional Raman Lidar technique I: temperature dependence and the calculation of atmospheric transmission", *Appl. Opt.*, this issue.

[2] R. M. Measures, *Laser Remote Sensing Fundamentals and Applications*, (Wiley-Interscience, New York, New York, 1984).

[3] G. Vaughan, D. P. Wareing, L. Thomas, V. Mitev, "Humidity measurements in the free troposphere using Raman backscatter", *Q. J. R. Meteor. Soc.*, **114**, 1471-1484 (1988).

[4] D. N. Whiteman, S.H. Melfi, and R.A. Ferrare, "Raman lidar system for the measurement of water vapor and aerosols in the earth's atmosphere", *Appl. Opt.*, **31**, No. 16, 3068-3082 (1992).

[5] U. S. Standard Atmosphere, 1976. NOAA document S/T 76-1562, National Oceanic and Atmospheric Administration, National Aeronautics and Space Administration, United States Air Force, Washington, DC 227 pp.

[6] D. Muller, K. Franke, F. Wagner, D. Althausen, A. Ansmann, J. Heintzenberg, "Vertical profiling of optical and physical particle properties over the tropical Indian Ocean with six-wavelength lidar 1. Seasonal cycle", *J. Geophys. Res. - Atmos.* 106: (D22) 28567-28575 (2001).

[7] D. Muller, D., K. Franke, F. Wagner, D. Althausen, A. Ansmann, J. Heintzenberg, G. Verver, "Vertical profiling of optical and physical particle properties over the tropical Indian Ocean with six-wavelength lidar 2. Case studies", *J. Geophys. Res. - Atmos.* 106: (D22) 28577-28595 (2001).

[8] P. B. Russell, T. J. Swissler, and M. P. McCormick,"Methodology for error analysis and simulation of lidar measurements", *Appl. Opt.*, **18**, 3783-3797 (1979).

[9] P. B. Russell, B. M. Morley, J. M. Livingston, G. W. Grams and E. M. Patterson, "Orbiting lidar simulations. 1: Aerosol and cloud measurements by an independent-wavelength technique", *Appl. Opt.*, **21**, 9,1541-1553 (1982).

[10] A. Bucholtz, "Rayleigh-scattering calculations for the terrestrial atmosphere". *Appl. Opt.*, 34, 15, 2765-2773 (1995).

[11] S. Chandrasekhar, *Radiative Transfer* (Dover, New York, 1960).

[12] A. Ansmann, M. Riebesell, C. Weitkamp, E. Voss. W. Lahmann, W. Michaelis, "Combined Raman Elastic-backscatter lidar for vertical profiling of moisture, aerosol extinction, backscatter, and lidar ratio, *Appl. Phys B.*, 55 (1), 18-28 (1992).

[13] R. A. Ferrare, R. A., S. H. Melfi, D. N. Whiteman, K. D. Evans, R. Leifer, "Raman lidar measurements of aerosol extinction and backscattering 1. Methods and comparisons." *J. Geo. Phys. Res.*, **103**, D16, 19663-19672 (1998).

[14] A. Deepak and L. H. Ruhnke, *Hygroscopic Aerosols*, (A. Deepak Publishing, 1984).

[15] W. F. Feltz, W. L. Smith, R. O. Knuteson, H. E. Revercomb, H. M. Woolf, H. B. Howell, "Meteorological applications of temperature and water vapor retrievals from the ground-based Atmospheric Emitted Radiance Interferometer (AERI)", *J. Appl. Meteor.*, 37: (9) 857-875 (1998).

[16] C. F. Bohren and B. A. Albrecht, *Atmospheric Thermodynamics*, Oxford University Press, New York, New York, 402 pp (1998).

[17] W. S. Heaps, J. Burris, J. A. French, "Lidar technique for remote measurement of temperature by use of vibrational-rotational Raman spectroscopy", *Appl. Opt.* 36: (36) 9402-9405 (1997).

[18] R. A. Ferrare, R.A., S.H. Melfi, D.N. Whiteman, K.D. Evans, F.J. Schmidlin and D.O'C. Starr, "A Comparison of Water Vapor Measurements made by Raman Lidar and Radiosondes", *J. Atmos. Ocean. Tech.*, **12**, 1177-1195 (1995).

[19] C. M. Penney and M. Lapp, "Raman-scattering cross-section for water vapor", *J. Opt. Soc. Am.*, **66**, 422-425 (1976).

[20] V. Sherlock, A. Hauchecorne, J. Lenoble, "Methodology for the independent calibration of Raman backscatter water-vapor lidar systems", *App. Opt.*, **38**, 27, 5816-5837 (1999).

[21] D. D. Turner, J. E. M. Goldsmith, "Twenty-four-hour Raman lidar water vapor measurements during the Atmospheric radiation Measurement program's 1996 and 1997 water vapor intensive observation periods", *J. Atmos. Ocean. Tech.*, 16: (8) 1062-1076 (1999).

[22] D. N. Whiteman, K. D. Evans, B. Demoz, D. O'C. Starr, D. Tobin, W. Feltz, G. J. Jedlovec, S. I. Gutman, G. K. Schwemmer, M. Cadirola, S. H. Melfi, F. J. Schmidlin, "Raman lidar measurements of water vapor and cirrus clouds during the passage of hurricane Bonnie", *J. Geophys. Res.*, 106, No. D6, 5211-5225 (2001).

[23] C. G. Wade, "An evaluation of problems affecting the measurement of low relative humidity on the United States radiosonde", *J. Atmos. Ocean. Tech.*, **11**, 687-700 (1994).

[24] P. M. Zhai, R. E. Eskridge, "Analyses of inhomogeneities in radiosonde temperature and humidity time series", *J. Climate*, **9**, 4, 884-894 (1996).

[25] B. M. Lescht, "Uncertainty in radiosonde measurements of temperature and relative humidity estimated from dual-sone sounds made during the September 1996 ARM Water Vapor IOP". In *Proceedings of the 10th Symposium on Meteorological Observations and Instrumentation.* Am. Meteorol. Soc., pp. 80-83, Phoenix, AZ, January 11-16, 1998 (1998).